Differential Equations and Dynamical Systems
https://doi.org/10.1007/s12591-023-00636-z

ORIGINAL RESEARCH

Local and Global Bifurcations in a Mechanochemical ODE Model for Cell Behavior

Cole Zmurchok[1] · **Matthew Sahota**[2] · **Wayne Nagata**[2] · **Eric N Cytrynbaum**[2]

Abstract
We study the dynamics of a two-variable mechanochemical model for GTPase signaling and cell tension using numerical bifurcation analysis, providing insight to the dynamics throughout parameter space. The model exhibits a wide range of local and global bifurcations, including three codimension-two bifurcations occurring along a locus of homoclinics. We use numerical bifurcation analysis and simulation to investigate these bifurcations. This analysis provides evidence for two rarely seen bifurcations: a neutral saddle homoclinic bifurcation and a non-central saddle-node homoclinic bifurcation. We expand the understanding of the dynamics of the mechanochemical model and provide a pedagogically useful example of a realistic but relatively simple model that exhibits a wide range of bifurcations.

Keywords Numerical bifurcation analysis · Mechanochemical model · Global bifurcations

Introduction

Bifurcation analysis is often an important step in understanding the dynamics of ordinary differential equation (ODE) models in mathematical biology throughout a parameter space. In the last decades, there has been increased interest in "mechanobiology"—where the mechanical properties and behaviors of cells are studied alongside traditional biochemical approaches. This interest has led to the development of an array of mechanochemical models for cell behavior, where the effects of both mechanics and biochemistry are jointly investigated [26]. One recent investigation used a nonlinear system of ODEs to explore how cell dynamics emerge from the interplay of GTPase signaling and

✉ Cole Zmurchok
czmurchok@gmail.com

Wayne Nagata
nagata@math.ubc.ca

Eric N Cytrynbaum
cytryn@math.ubc.ca

[1] Department of Physics and Astronomy, Vanderbilt University, Nashville, TN, USA

[2] Department of Mathematics, The University of British Columbia, Vancouver, BC, Canada

Published online: 29 March 2023

cell tension [32]. A numerical bifurcation analysis played a key role in this study, as it outlined parameter regimes where the cell could exhibit different behaviors (oscillatory vs. contracted vs. expanded). However, this bifurcation analysis was limited to one parameter. Here, we expand the analysis to two key model parameters, and study the local and global bifurcations that occur in the parameter space.

The single-parameter bifurcation analysis of Zmurchok et al. [32] focused on codimension-one bifurcations. This was sufficient for the purposes of their investigation; however, a complete mathematical investigation of the model's dynamics throughout parameter space remains unfinished. Our investigation began when we noted the possibility of a rare codimension-two bifurcation involving a homoclinic solution and saddle-node bifurcation in the model from Zmurchok et al. [32]. To investigate this, we expanded the bifurcation analysis to two parameters and sought to characterize the global and local codimension-two bifurcations.

Our investigation, besides providing a more complete mathematical analysis of a mechanochemical model, is motivated by two other observations. First, several recent studies by Bui et al. [2], Tambyah et al. [29], and Link et al. [20] have adapted the model from Zmurchok et al. [32]. Further investigations may benefit from a complete bifurcation analysis of the original model. Second, while there is an abundance of examples of mathematically interesting global codimension-two bifurcations taught in advanced dynamical systems courses with applications in neuroscience or ecology, few (perhaps no) examples are related to contemporary mechanochemical models. Our investigation here could be used as such an example in a classroom setting since we will use numerical bifurcation analysis alongside numerical simulations and phase-plane analysis to study codimension-two bifurcations.

We begin our study with a two-parameter numerical bifurcation analysis, revealing Hopf and saddle-node local codimension-one bifurcations (see Kuznetsov [17] for an overview of bifurcation theory). For certain parameter values, a limit cycle terminates at a saddle-node steady state, in a codimension-one bifurcation known as a saddle-node on an invariant circle (SNIC). At this bifurcation, there is a solution that is homoclinic to a saddle-node steady state (note that Homburg and Sandstede [14] review homoclinic and heteroclinic bifurcation theory for autonomous vector fields). We also find several local codimension-two bifurcations: a generalized Hopf, cusp bifurcations of periodic solutions, a Bogdanov-Takens (BT) bifurcation. Finally, we find two global codimension-two bifurcations: a neutral-saddle homoclinic bifurcation, and a non-central saddle-node homoclinic (NCH) bifurcation.

We focus our analysis on the BT bifurcation and the two global bifurcations. While BT bifurcations are relatively common and often studied in models, we include it in our focus since it is the "birthplace" of a homoclinic solution that is a key ingredient to the two less common global codimension-two bifurcations.

At a neutral-saddle homoclinic bifurcation, the stability of the homoclinic orbits and bifurcating limit cycles change [6, 14, 18, 25]. Moreover, theory predicts that a curve of saddle-node bifurcations of periodics has exponentially flat tangency to the bifurcation curve of saddle homoclinics [5] at such a bifurcation point.

At the non-central saddle-node homoclinic bifurcation, the solution that is homoclinic to the saddle-node steady state leaves the steady state tangent to the central direction and approaches tangent to the non-central direction [5, 7, 14, 22, 28]. Note that the NCH bifurcation has also been named a "saddle-node separatrix loop" bifurcation [15, 22, 28], and appears in several models with application to neuroscience such as the

Morris-Lecar [24], Chay-Cook [4], Wilson-Cowan [31], and Tsaneva-Atanasova [9, 30] models and in ecological models as well [1, 17].

To confirm predictions of our numerical bifurcation analysis we provide representative phase-plane examples throughout parameter space, and detailed numerical simulations near the NCH point. Numerical continuation of homoclinic solutions requires some care when using numerical bifurcation software. Considerable effort has been made in developing software and numerical methods to continue homoclinic solutions [3, 10] and to identify NCH bifurcations in models such as Morris-Lecar [11, 21] and cell-cycle models [12]. Because of this difficulty, we use phase-plane analysis and simulations in conjunction with numerical bifurcation analysis software to support our conclusions. Our analysis thus provides evidence for these two bifurcations: a neutral saddle homoclinic bifurcation and a non-central saddle-node homoclinic bifurcation. Overall, our analysis expands the understanding of the dynamics of the mechanochemical model and provides a pedagogically useful example of an analysis of a realistic model exhibiting a wide range of bifurcations.

Methods

We analyze the GTPase-Tension model first introduced by Zmurchok et al. [32]. This model was designed to provide a simple description of the interplay between cell signalling and cell mechanics. It was used to generate a variety of cell behaviors, ranging from large, relaxed cells, to oscillatory cells that dynamically change length, to small, contracted cells. We use numerical bifurcation analysis to classify and analyze a wide variety of local and global bifurcations in the two-dimensional ODE model of cell behaviour that couples cell mechanics and biochemical signaling.

Our numerical bifurcation approach uses standard numerical continuation methods and free software such as XPPAUT (available from https://sites.pitt.edu/~phase/bard/bardware/xpp/xpp.html).

GTPase-Tension Model

GTPase signals are responsible for regulating a cell's shape and size by modulating the cytoskeleton [27] which is the mechanical infrastructure of the cell. Zmurchok et al. [32] coupled cell mechanics back to GTPase signaling through cell tension.

In their model, the dynamics of a cell's size, where size is measured by end-to-end length L, is determined by a mechanical spring-dashpot (a Kelvin-Voigt element) for the cytoskeleton in the overdamped low Reynolds number limit:

$$\frac{dL}{dt} = -\varepsilon(L - L_0) \tag{1}$$

The parameter $\varepsilon = 2k/\lambda$ is small and is defined as the ratio of the spring constant k to the viscosity λ.

The Rho-family GTPases are known to be central regulators of signaling networks in eukaryotic cells. GTPases exist in active and inactive states, and when activated, Rho GTPase signals to downstream effectors that eventually result in myosin-induced cell

contraction. Thus high (Rho) GTPase activation leads to cytoskeleton contraction and hence a shorter cell rest length. In the model, the spring rest length, L_0 is defined to be

$$L_0 = L_0(G) = \ell_0 - \phi \frac{G^p}{G_h^p + G^p}. \tag{2}$$

where G is the GTPase activation level. In the "sharp-switch limit" ($p \to \infty$), GTPase activity reduces the cell's rest length from ℓ_0 to $\ell_0 - \phi$ whenever $G > G_h$.

The feedback from cell length to GTPase dynamics comes through the spring tension which is proportional to $\Delta L = L - L_0(G)$. The equation for GTPase concentration is

$$\frac{dG}{dt} = \left(b + f(\Delta L) + \gamma \frac{G^n}{1 + G^n}\right)(G_T - G) - G, \tag{3}$$

where the first term is the GTPase activation rate and the second is the inactivation rate. The tension-dependent activation term is

$$f(\Delta L) = \frac{\beta}{1 + \exp[-\alpha \Delta L]}. \tag{4}$$

On the time-scale of GTPase signaling, a common assumption is that the total amount of GTPase is constant, G_T [13, 23, 32]. These observations explain the main features of the model's equation for $G(t)$ — inactivated GTPase ($G_T - G$) becomes activated with rate coefficient in parenthesis, ($b + f(\Delta L) + \ldots$) and active GTPase becomes deactivated at a rate linear in G. The activation rate coefficient contains the basal activation rate parameter b, positive feedback from cell tension and from GTPase signaling to itself (through the hill function with amplitude γ, half-maximum 1, and exponent n).

In the absence of feedback from tension ($\beta = 0$), the GTPase equation can exhibit bistability over a range of the basal activation rate b, thus explaining how GTPase signaling can be switched "on" or "off" as parameters or initial conditions change. Bistability also permits hysteresis which allows the system to act as a relaxation oscillator when the activation rate is slowly varied up and down.

To give a physical sense of the dynamics, consider a situation in which GTPase activation rises in a resting cell by some external stimulus. Increased GTPase activation shortens the cell rest length creating tension in the cell ($\Delta L > 0$). This tension simultaneously induces contraction which tends to relieve tension but also stimulates GTPase activation which further shortens the rest length driving an increase in tension. This conflicting feedback, depending on parameters, can result in a variety of dynamical behaviors, including large or small cells or a relaxation oscillation where the GTPase oscillates between high and low values and the cell's length oscillates between small and large values, respectively.

Numerical Bifurcation Approach

We focus our investigation on the bifurcation parameters b and β, since these parameters broadly control the overall level of GTPase activity and the strength of the feedback from cell mechanics. We fix the values of the other parameters to match those used in Zmurchok et al. [32]: $\gamma = 1.5$, $G_T = 2$, $\ell_0 = 1$, $\phi = 0.75$, $G_h = 0.3$, $\varepsilon = 0.1$, $\alpha = 10$, and $n = p = 4$. For our analysis, we used freeware XPPAUT, MatCont [8] for MATLAB (MATLAB and

Statistics Toolbox Release 2020b, The MathWorks, Inc., Natick, Massachusetts, United States), and Python. Code is available at https://www.github.com/zmurchok/GTPase-tension-bifurcation.

Results

Bifurcation Analysis

We used numerical bifurcation analysis to extend the one-parameter bifurcation diagram in Zmurchok et al. [32] to the $b\beta$-plane. Our analysis recapitulates the basic features of the model. Namely, that there is a large region of bistability (Figure 1A) between two codimension-one local saddle-node (SN) bifurcations that run roughly parallel through the $b\beta$-plane, and there is a codimension-one local Hopf (H) bifurcation that results in limit cycles (periodic solutions). In the parameter region between the two SNs, there are two stable solutions to the left/above the Hopf curve (H): (1) a high G, low L steady-state, and (2) a low G, and high L steady-state, that correspond to a contracted cell with large GTPase activity, and a relaxed cell with little GTPase activity, respectively. Below/right of the Hopf curve, the low-G-high-L steady state is unstable, having lost stability at the Hopf. For parameter values between the two SN there is in addition a third steady state, an unstable saddle, with intermediate G and L values. In the bottom-left of Figure 1A,

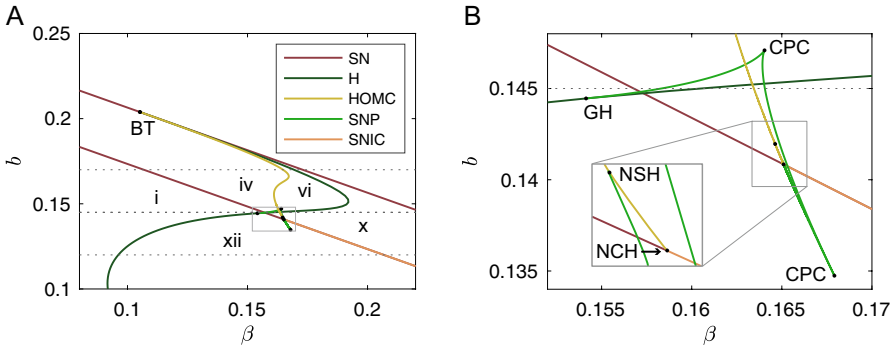

Fig. 1 **A** Two-parameter bifurcation diagram in β and b. Two loci of saddle-node bifurcations (SN, dark red and orange) run roughly parallel to each other throughout the diagram. A locus of saddle homoclinic bifurcations (HOMC, gold) extends between a pair of codimension-two bifurcations, from a Bogdanov-Takens bifurcation (BT) on the right/upper SN to a non-central saddle-node homoclinic bifurcation (NCH) on the left/lower SN. A locus of Hopf bifurcations (H, dark green) winds its way from the BT across the diagram going through a codimension-two generalized Hopf bifurcation (GH) on the way. Roman numerals label *regions* that are enclosed by bifurcation curves. **B** A close-up of the region around the NCH (shown in (A) as the grey box). The SN and HOMC collide at the NCH. Above/left of the NCH, the SN is a simple saddle-node bifurcation (dark red). Below/right of the NCH, the SN is a saddle-node on an invariant circle bifurcation (SNIC, orange). Near this, a locus of saddle-node bifurcations of periodic solutions (SNP, green) extends from the GH, through two codimension-two cusp bifurcations (CPC), and finally terminating on the locus of hyperbolic saddle homoclinics (HOMC) at the point where the hyperbolic saddle is neutral, a codimension-two neutral-saddle homoclinic bifurcation (NSH). The segment of the green SNP curve near its terminal point Y is extremely close to the gold HOMC curve and is obscured by it if plotted to scale — the inset sketch (modified by hand to separate green and gold curves for clarity) in Figure 1B shows this detail

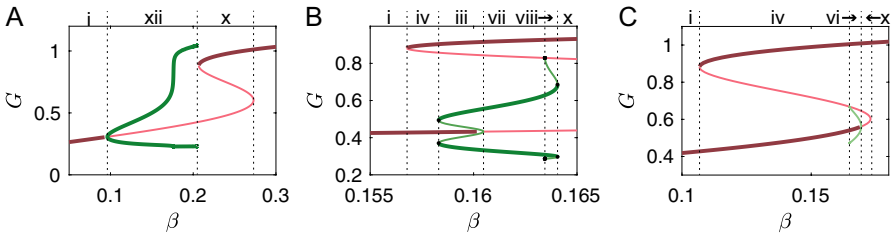

Fig. 2 One-parameter branching diagrams in β and G, corresponding to the horizontal dotted lines in Fig 1A (A: $b = 0.12$; B: $b = 0.145$; C: $b = 0.17$). Stability is indicated by line thickness (thick: stable; thin: unstable) with periodic solutions (maximum and minimum G values) in green and steady states (G values) in red. Vertical dashed lines on each panel denote where bifurcations occur, corresponding to the boundaries of regions defined by Roman numerals in Figure 3 (note that some regions are not labelled). Panel A illustrates how a branch of stable periodic solutions arises at a supercritical Hopf bifurcation and terminates in a SNIC (at the boundary between regions xii and x). Panel B illustrates some of the intricate detail near the GH point: a subcritical Hopf bifurcation gives rise to a branch of unstable periodic solutions that goes through two saddle-node bifurcations of periodic solutions (giving multiple periodic solutions in regions iii and viii), and eventually terminates in a saddle homoclinic bifurcation. Panel C illustrates the behavior of the system closer to the BT point where an unstable periodic solution is born through a subcritical Hopf bifurcation and terminates in a saddle homoclinic bifurcation

the low-G-high-L steady state is the only one present and can be either stable or unstable depending on parameters (stable to the left of the Hopf curve, unstable to its right), and in the top-right, the high-G-low-L steady-state is the only one and it is stable. The presence of the bistability and limit cycles can be seen in Figure 2A, where a one-parameter bifurcation diagram in β is plotted for $b = 0.12$ (corresponding to the dashed line at the bottom of Figure 1A). This basic structure of two saddle-node bifurcations and a Hopf bifurcation can be seen throughout most of the $b\beta$-plane with the Hopf bifurcation disappearing above the BT bifurcation in Fig. 1) and appears in all panels of Figure 2. The location and types of bifurcations related to the limit cycles vary with the parameters.

The stability and subsequent bifurcations of the limit cycles emanating from the Hopf bifurcation point vary with the basal activation rate b. For small b, the Hopf bifurcation is supercritical and produces a stable limit cycle for various β values (Figure 2A). As β increases, this limit cycle terminates on the saddle-node at the lower β value, in a codimension-one bifurcation known as a saddle-node on invariant circle, or SNIC (Figure 1, orange curve), where the saddle-node bifurcation occurs with a homoclinic solution. The SNIC bifurcation is also called a central (generic) saddle-node homoclinic bifurcation. The Hopf bifurcation changes criticality at $b \approx 0.1445$, where there is a codimension-two generalized Hopf (GH) bifurcation. For b above this value, the Hopf bifurcation is subcritical and produces an unstable limit cycle near the Hopf bifurcation (Figure 2B and C). For larger b, the subcritical Hopf bifurcation occurs very close to the SN at the larger β and the unstable limit cycle terminates in a codimension-one (non-neutral, generic) saddle homoclinic bifurcation (Figure 2C). Finally, for $b \approx 0.2039$, the Hopf bifurcation disappears at a codimension-two Bogdanov-Takens (BT) bifurcation (Figure 1A). Vertical dashed lines in Figure 2 illustrate where different bifurcations occur, and correspond to the boundaries of *regions* that are defined by Roman numerals in Figure 3. Later, we will examine the phase plane of the system with parameters in each of these regions to better understand the local and global bifurcations throughout parameter space.

We find that the GTPase-tension model exhibits several codimension-two bifurcations: a local generalized Hopf (GH) bifurcation, local cusp bifurcations of periodic solutions, a

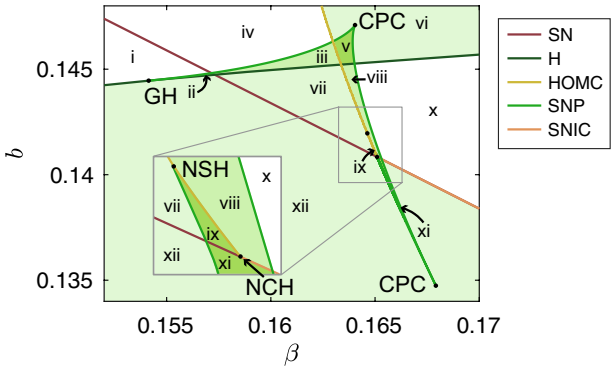

Fig. 3 Annotated two-parameter bifurcation diagram in β and b with regions marked by Roman numerals. Shading indicates the number of periodic solutions in each regions: white - no periodic solutions; light, intermediate, and dark green - one, two, and three periodic solutions, respectively. Codimension-two bifurcation points are marked by capitalized letters: GH - generalized Hopf bifurcation; CPC - cusp bifurcations (of periodics); NSH - neutral saddle homoclinic; NCH - non-central saddle-node homoclinic. Inset sketch: cartoon of bifurcation curves and regions vii, viii, and ix. Region ix is actually extremely narrow but we manually moved the NCH point for clarity; the green and gold curves would actually overlap at the scale shown, consistent with the expected exponential tangency

local Bogdanov-Takens (BT) bifurcation, a global neutral saddle homoclinic bifurcation, and a global non-central saddle-node homoclinic bifurcation (NCH). At the GH bifurcation (Figure 1B), the criticality of the Hopf bifurcation flips from supercritical to subcritical, and a locus of SNP bifurcations extends from this point. The SNP curve (green in Figure 1) encounters two cusp bifurcations (CPC points in Figure 1B) before terminating at a point (labelled NSH in Figure 1) on the locus of hyperbolic saddle homoclinics (HOMC, gold in Figure 1).

Codimension-Two Bifurcations with Homoclinic Solutions

Arguably the most interesting feature of the bifurcation diagram is the presence of a non-central saddle-node homoclinic bifurcation (labelled NCH in Figure 1) at the junction between the lower SN and the locus of homoclinics. This codimension-two global bifurcation is a foil to the BT bifurcation, with the HOMC arising at the BT on one SN, and ending at the NCH on the other SN. In fact, homoclinic solutions do not actually disappear at the NCH, but rather change, from homoclinics to hyperbolic saddle steady states, into homoclinics to non-hyperbolic saddle-node steady states (SNIC). We made an animation illustrating how the homoclinic solutions change as parameters are varied in the $b\beta$-plane along the gold HOMC curve, through the NCH, and then along the orange SNIC curve (Supplemental Video 1). Given the centrality of the homoclinic bifurcations to the bifurcation structure of the system, we focus on the three codimension-two bifurcations involving the homoclinic solutions.

Bogdanov-Takens Bifurcation

The Bogdanov-Takens (BT) bifurcation [17] is a relatively common codimension-two bifurcation at which a locus of limit cycles disappears through the collision of Hopf and

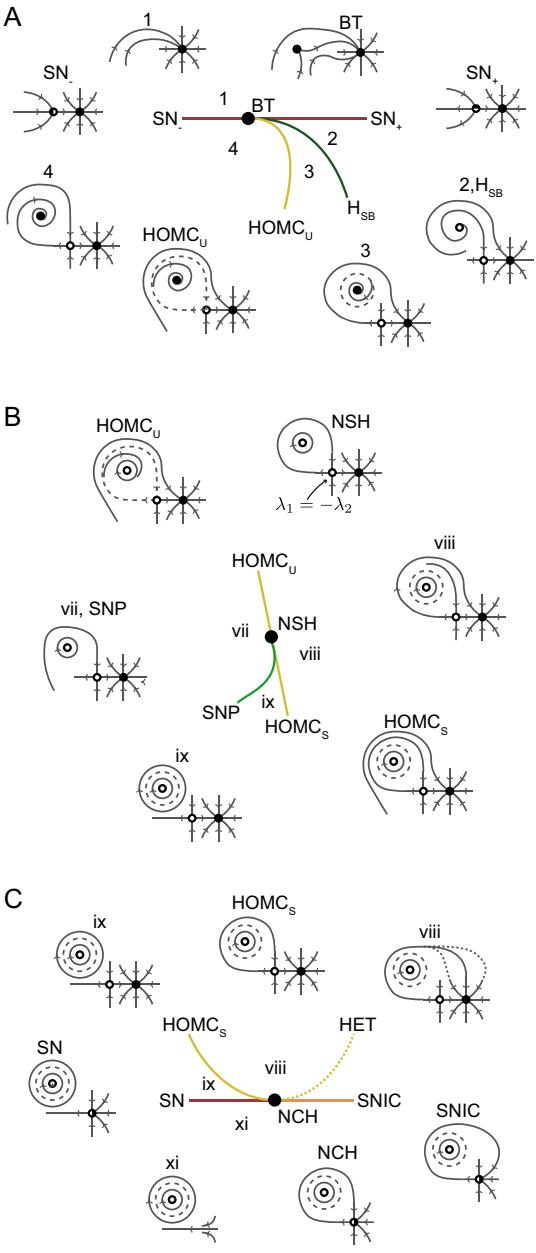

Fig. 4 Cartoon of bifurcations and phase-plane behavior involving homoclinic orbits in the GTPase-tension system. **A** Unfolding of the Bogdanov-Takens bifurcation. **B** Unfolding of the neutral saddle homoclinic bifurcation, **C** Unfolding of the non-central saddle-node homoclinic bifurcation. Each panel illustrates the codimension-two bifurcation point of interest (points labelled BT, NSH, and NCH) and the corresponding bifurcation curves. Surrounding each cartoon are sketches of the phase-plane behavior of the GTPase-tension model. Each phase-plane sketch is labelled and corresponds to a region near the codimension-two bifurcation or to a codimension-one bifurcation curve emerging from it. Grey curves and small arrows illustrate trajectories and the flow direction while steady states are indicated by small dots (stable: filled dot; unstable: unfilled dot; semi-stable: half-filled dot). Stable limit cycles and homoclinics are shown as solid lines while unstable limit cycles and homoclinics are shown with dashed lines. The phase-plane along the non-bifurcation curve HET (dotted gold) in panel C corresponds to the cartoon labelled viii, where the large loop heteroclinic connection from the saddle approaches tangent to the fast direction of the stable node. Alternative arrangements (for parameter values in region viii on either side of the curve HET) of the heteroclinic connection are illustrated in the same phase-plane cartoon via dotted lines (see Figure 5 for details)

homoclinic bifucations. In the present model, the BT bifurcation occurs on the the upper SN curve for small β and large b as in Figure 1A. At the BT point, both eigenvalues of the linearization at the steady-state are zero — the BT bifurcation is also known as a (generic) double-zero bifurcation. In Figure 4A, we present a cartoon of the BT including the bifurcation curves and sketches of the phase-plane behavior along each bifurcation curve and in the regions between curves. Each bifurcation curve is colored as in Figure 1 and each

phase plane illustrates solutions (grey curves with arrows showing the flow direction) as well as steady states and their stability (stable, solid dot; unstable, empty dot; semi-stable, half-filled dot). Note that the homoclinic and Hopf curves collide at the BT point with limit cycles existing for parameter values in the region between these two curves. In the GTPase-tension model, the homoclinic solutions are unstable for parameters near the BT, with solutions that start at $t = 0$ in the interior of the homoclinic loop close to the homoclinic evolving away from the homoclinic and approaching as $t \to \infty$ the stable node or spiral (large G, low L) that exists inside the homoclinic loop. Similarly, the Hopf bifurcation is subcritical near the BT and it gives rise to unstable limit cycles as parameters are varied between region 2 and 3 in Figure 4A.

Neutral Saddle Homoclinic Bifurcation

As the parameter b is decreased from the BT value along the locus of saddle homoclinic bifurcations (HOMC, gold curve in Figure 1 and Figure 3), the eigenvalues, λ_1, λ_2, of the linearization at the saddle steady-state satisfy $\lambda_1 + \lambda_2 > 0$. This implies that the homoclinic solutions to the saddle, and the bifurcating limit cycles for nearby parameter values, are unstable. Moreover, the unstable limit cycles bifurcate to the right of the HOMC curve, i.e., as the parameter β increases from a critical value on the HOMC curve.

The expression $\lambda_1 + \lambda_2$ is equal to the trace of the linearization matrix, or the divergence of the vector field, at the hyperbolic saddle steady-state. As b decreases from the BT value along HOMC, eventually the value of the trace decreases to zero, at the point labelled NSH, where $b \approx 0.1419$. Here the hyperbolic saddle is neutral, with $\lambda_1 = -\lambda_2$. As b decreases further, below the value at NSH, the trace at the saddle is negative and the homoclinic solutions to the saddle and the corresponding bifurcating limit cycles are stable. The stable limit cycles bifurcate to the left of HOMC, as illustrated in Figure 4B.

The point NSH corresponds to a codimension-two neutral saddle homoclinic bifurcation [6, 14, 18, 25], where the trace of the linearization at the saddle changes sign, and hence the stability of the homoclinic orbits and bifurcating limit cycles change. The locus of saddle-node bifurcations of periodic solutions (SNP, green curve in Figure 1) extends from the generalized Hopf point (labelled GH), through two cusp bifurcations of periodics (labelled CPC), and terminates on HOMC at NSH, accounting for the change in stability and direction of the limit cycles that bifurcate from the homoclinic solution for parameters near the bifurcation point NSH.

At a neutral saddle homoclinic bifurcation point, the SNP curve has an exponentially flat tangency with the HOMC curve [6]. For b slightly less than the value at NSH, the SNP curve is to the left of the HOMC curve, but extremely close, due to the exponential flatness at the intersection point NSH. This makes region ix, between SNP and HOMC, very narrow. For example, if $b = 0.1410$, then the β values corresponding to region ix are confined to a tiny interval, between approximately 0.16502938 and 0.16502941, and the stable limit cycle that bifurcates from the homoclinic solution is extremely close to an unstable limit cycle that is just inside the stable one (Figure 6).

Non-Central Saddle-Node Homoclinic Bifurcation

As the parameter b is decreased along the HOMC curve below the value at the point NSH, the trace of the linearization at the saddle remains negative. Eventually as b is decreased further to $b \approx 0.14084$, the positive eigenvalue at the saddle shrinks to zero. At this point

in the parameter plane, labelled NCH in Figure 1B and Figure 3, the steady-state associated with the homoclinic solution is a non-hyperbolic saddle-node, whose linearization has a zero eigenvalue and a negative eigenvalue. The solution that is homoclinic to the saddle-node steady-state leaves tangent to the central direction (associated with the zero eigenvalue), and approaches tangent to the non-central direction (associated with the non-zero, negative, eigenvalue) which is transverse to the central direction. A phase-plane for parameter values at the NCH is illustrated in Figure 4C. Amongst all saddle-node homoclinic orbits, the orbit for parameter values at NCH is a non-generic case, and it corresponds to a codimension-two non-central saddle-node homoclinic bifurcation [5, 7, 14, 22, 28].

At the NCH bifurcation point, the HOMC curve terminates on one of the SN curves, a locus of parameter values where the model has a saddle-node steady state. To the left of the NCH point (decreasing β), the locus of saddle-nodes (dark red) corresponds to a codimension-one local saddle-node bifurcation. To the right of the NCH, the locus of saddle-nodes (orange) corresponds to a codimension-one global saddle-node on invariant circle (SNIC) bifurcation. For parameter values on the SNIC curve, there is a homoclinic orbit that both leaves and approaches the saddle-node steady-state tangent to the central direction, and therefore the homoclinic solution together with the saddle-node steady-state form a smooth invariant circle. The SNIC is the generic case for a saddle-node homoclinic solution and is illustrated in Figure 4C.

It is possible to predict the presence of an NCH bifurcation on the basis of nullcline patterns [15, 16] in two-dimensional systems, which are similar in several models, including the GTPase-tension model, but we are aware of only a few cases where an NCH bifurcation is identified numerically [3, 10–12]. We used XPPAUT and MatCont to numerically identify the NCH in the GTPase-tension model; however, numerical errors associated with computing homoclinics in both bifurcation software packages seemed too large to visually confirm the quadratic tangency of the HOMC and SN-SNIC curves predicted by Schecter [28].

There is an additional ("non-bifurcation") curve of parameter values associated with the NCH bifurcation. We label this curve HET in Figure 4C since it characterizes special, non-generic heteroclinic connections from the saddle to the nearby node for parameter values in region viii. For parameter values along the HET curve, the left branch of the unstable manifold of the saddle forms large loop around the phase plane and as $t \to \infty$ makes a heteroclinic connection to the strong stable manifold of the node (tangent to the fast direction, associated with the more negative of the two negative eigenvalues of the linearization at the node). In all of region viii, the right branch of the unstable manifold of the saddle also makes a heteroclinic connection with the node, in this case to the weak manifold. This connection is generic and does not change with small changes in parameter values in any interesting way.

The HET curve is not a bifurcation boundary and does not affect the topological equivalence of the phase portraits for parameter values in region viii, yet the large loop heteroclinic connection falls on different "sides" of the strong stable manifold of the node when parameters are chosen on either side of this HET curve. To further confirm that our point NCH is indeed an NCH bifurcation we sought numerical evidence for this HET curve. We fixed b and chose values of β near the NCH. For each parameter value, we numerically found the saddle and node steady states and the eigenvalues and eigenvectors of the linearizations at both steady states, and we numerically integrated the GTPase-tension model with initial conditions on the left branch of the unstable direction of the saddle. We plot a portion of the phase-plane near the saddle and node steady states in Figure 5. For (b, β) in region ix, we observe that the solution approaches a stable limit cycle (panel A). As β

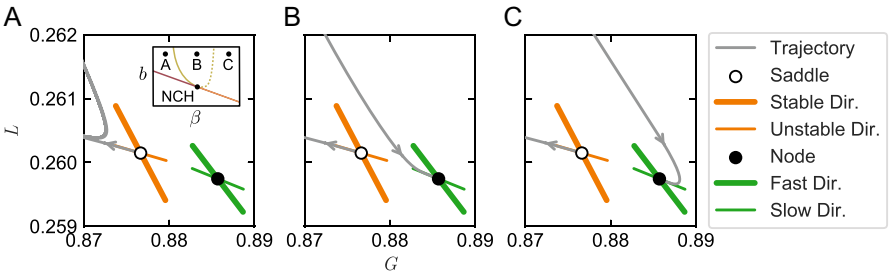

Fig. 5 Numerically calculated phase portraits near the NCH as in Figure 4C in region viii. A single trajectory (grey curve) starting on the unstable direction of the saddle equilibrium (unfilled dot) loops around the phase plane before turning to a limit cycle (panel A) or becoming a heteroclinic connection to the stable node (black dot) in panels B and C. Stable and unstable directions (Dir; i.e., eigenvectors) are shown for the saddle, and fast and slow directions are shown for the stable node. Inset cartoon illustrates how the parameter values change in each panel and their relation to the homoclinic curve (solid gold curve), the SN (dark red) and SNIC (orange) curves: $b = 0.14088$ throughout, and $\beta = 0.1650804$, 0.1650806, 0.1650810 in panels A, B, and C, respectively. Note that the heteroclinic connection changes position relative to the fast direction of the node as the parameter β increases. The change in position is consistent with the bifurcation diagram of the NCH illustrated in Figure 4 and suggests the existence of a large loop heteroclinic connection from the saddle that approaches the node tangent to the fast direction for a value of b intermediate to the latter two values above

increases, the parameter values (b, β) cross the HOMC curve into distict viii, and we see the solution forms a heteroclinic connection to the node (panels B and C). We observe that as β increases, this heteroclinic connection switches from the "left" to the "right" side of the fast direction (tangent to the strong stable manifold) for the node (compare panel B and panel C). Assuming continuity with respect to parameters and accuracy of the simulations, this switching implies that there are values of (b, β) for which the heteroclinic connection approaches exactly tangent to the fast direction of the node. We remark that the HET curve appears to fall very close to the HOMC curve and that it may be possible to approximate the HET curve using a bisection method (e.g., for each b, approximate the β value where the heteroclinic solution switches sides as in panels B and C).

Phase-Plane Analysis

To further explain the dynamics and bifurcations observed in the $b\beta$-plane, we plotted phase portraits for a wide range of parameter values using both numerical simulation and computed periodic or homoclinic solutions from continuation.

Dynamics in Each Region

We focus on several of the regions labelled in Figure 3 that border the homoclinic curve, and plot phase portraits in Figure 6. Each phase portrait illustrates the steady states and periodic solutions alongside their stability as well as the stable and unstable manifolds corresponding to steady states classified as saddles. The coloring scheme matches that of the other figures — stable steady states and limit cycles are shown with bold lines in red and green respectively; unstable steady states and limit cycles are shown with thin lines in red and green respectively. We illustrate saddles with a diamond symbol and plot selected parts of the stable manifold in black and unstable manifold in grey. For example, the first

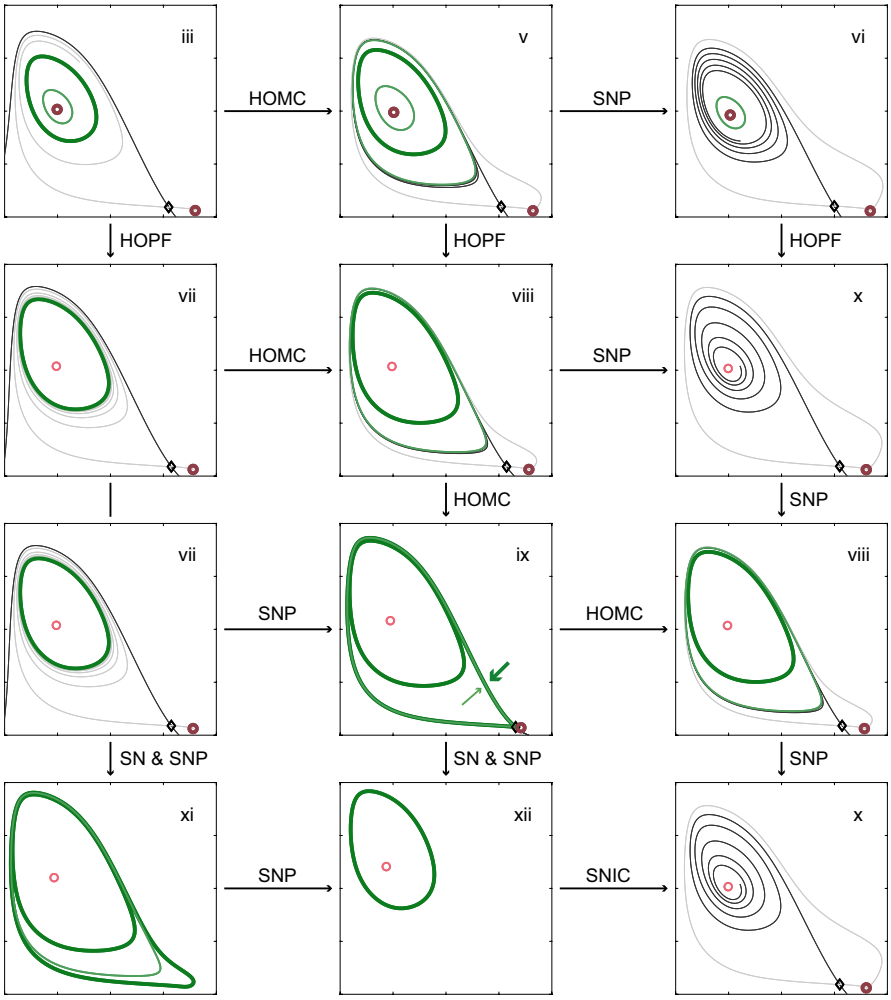

Fig. 6 Selected L versus G phase-planes illustrating the dynamics in various regions (identified by Roman numerals) roughly corresponding to moving downwards along the locus homoclinic bifurcations towards the NCH in Figure 3. Periodic solutions are shown in green along with stability (thick, dark: stable; thin, light: unstable), stable steady states are marked with thick dark red circles and unstable steady states with thin light red circles, saddles are denoted with a black diamond, and the black and grey trajectories indicate the stable and unstable manifolds, respectively, of the saddle. Note that the stable and unstable periodic solutions are very close in region ix and are thus indicated with arrows. Annotated arrows between diagrams indicate the bifurcation(s) that occur as β and b parameters are varied to move between regions

panel of Figure 6 (labelled iii) shows the phase-plane for selected parameters in region iii (Figure 3). For these parameter values, we expect there to be three steady states (since we are in the bistable parameter regime between the SNs) as well as two periodic solutions (one stable and one unstable since the Hopf bifurcation is subcritical for these parameters). Indeed, we observe two stable steady states separated by a saddle, with the stable manifold of the saddle acting as a separatrix. Solutions above the stable manifold tend to the high G, low L steady-state, while other trajectories approach the stable limit cycle. Solutions with

initial conditions within the smaller unstable periodic solutions tend to the high L, low G steady-state.

We designed the layout of Figure 6 to help the reader understand the bifurcations that occur along the locus of saddle node homoclinics (HOMC; gold curve in Figure 3 starting from the BT point down towards the NCH. Overall, the rows and columns of Figure 3 correspond to moving horizontally or vertically, respectively, through the regions in Figure 3. For example, the first row of panels corresponds to a roughly horizontal slice through the $b\beta$-plane moving through regions iii, v, and vi. Labelled arrows in Figure 6 explain the various bifurcations that occur as parameters are varied through regions and help the reader decipher the meaning of the various bifurcations. For example, moving vertically in the diagram in Figure 3 from region iii to vii requires a Hopf bifurcation. This Hopf bifurcation can easily be seen from the phase-planes as the small amplitude unstable periodic solution disappears when parameters are varied from region iii to vii. Note that the SNP occurs very close to the saddle node homoclinic bifurcation as parameters vary from regions vii–ix–vii as illustrated in the inset sketch in Figure 1B. The behavior in this relatively small portion of parameter space can be observed in the phase planes shown in the third row of Figure 6. In region vii, there is only one stable periodic solution. As β increases to parameter values in region ix, a saddle node of periodics bifurcation occurs. Thus, in region ix, there are three periodic solutions, with the largest amplitude solutions (one stable and one unstable) nearly superimposed as indicated by the light green and dark green arrows in the panel of Figure 6 corresponding to region ix (see also Section 3.2). Finally, as β increases further, the large amplitude stable periodic solution forms a saddle node homoclinic and the phase plane thus appears as shown in region vii, where there are two periodic solutions (one stable and one unstable).

Discussion

In this study, we completed a two-parameter bifurcation analysis of the mechanochemical model developed by Zmurchok et al. [32]. We found a wide variety of local and global bifurcations depending on the two key parameters in the system: b and β. Biologically, these two parameters characterize the overall activity of GTPase signaling within the cell (due to the basal activation rate b), as well as the strength of mechanics-based feedback (β) from the cell's length to the GTPase signaling. Our bifurcation analysis here extends the initial analysis that only focused on β [32] to a wider region in parameter space. Besides the extension of the analysis into a wider parameter space that should interest those studying the dynamics of this mechanochemical model or its variants in the context of single and collective cell behavior such as the work by Bui et al. [2],Link et al. [20],Tambyah et al. [29], there are two other purposes to our investigation. First, we sought a comprehensive numerical continuation, phase-plane analysis, and overview of the relevant theory for the global codimension two bifurcations that occur in these models (Bogdanov-Takens, neutral saddle homoclinic, and non-central saddle-node homoclinic bifurcations). This investigation adds to the list of dynamically interesting models exhibiting such a non-central saddle-node homoclinic bifurcation [3, 4, 10–12, 15, 17, 19, 21, 28, 31], yet is the first, to our knowledge, documented example in a biophysically realistic mechanochemical model. Second, we expect these results to be of interest to those teaching advanced courses on nonlinear dynamical systems as a contemporary and biologically realistic example.

The initial investigation of the mechanochemical model studied here was restricted to a bifurcation analysis in the parameter β [32]. There, the authors sought to explain cell behavior as a function of this parameter that encodes the strength of feedback from cell mechanics on to regulatory cell signaling. Our investigation started when we noticed the possibility of a codimension two bifurcation involving a homoclinic solution and saddle-node bifurcation in that model, and thus sought to provide numerical evidence for this NCH point in a two parameter bifurcation analysis.

As a first step, we used the numerical continuation software MatCont in order to perform a two parameter bifurcation analysis. We found that the mechanochemical model had a standard array of codimension-one local bifurcations including saddle-node, Hopf, and saddle-node of periodic bifurcations as well as commonly found local codimension-two bifurcations such as a generalized Hopf, cusps of saddle-nodes of periodics, and a Bogdanov-Takens bifurcation. We also found several mathematically interesting global codimension-two bifurcations involving a locus of saddle-node homoclinic bifurcations, including a non-central saddle-node homoclinic bifurcation (NCH in Figure 1) and a neutral saddle homoclinic bifurcation (NSH in Figure 1). We confirmed our numerical bifurcation results using the XPPAUT package, which incorporates the AUTO numerical continuation software. We found XPPAUT easier to use than MatCont, but less powerful. With both packages, we found continuing homoclinic orbits near global bifurcations to be less than straightforward and it is helpful to know beforehand what you are looking for.

We next focused our analysis on the theory and numerical computation of these global codimension-two bifurcations. Our results agree with the theoretical characterization of these bifurcation points, as we compared the theoretical predictions (Figure 4) with detailed numerical investigations and comprehensive phase-plane analysis in each *region*. The purpose of this analysis was two-fold. First, we used the phase-plane analysis (Figure 6) to confirm the theoretical characterization of the BT, neutral saddle homoclinic bifurcation, and the NCH (Figure 4). Second, we provide the phase-plane analysis to characterize the cell dynamics in terms of cell size, L, and cell GTPase signaling, G in each region. This analysis reveals how slight changes in parameter space, especially in areas of the parameter space where the bifurcation curves are fairly close together, can lead to different cell dynamics (e.g., losing or gaining periodic solutions). Although many of the parameter regions with interesting dynamical behavior are extremely small, this analysis reveals insight to the expected cell dynamics predicted by this model (large relaxed cells, small contracted cells, or cells that periodically change size). The small regions in parameter space on cell dynamics are unlikely to be observed in real cells, owing to the inherent randomness that would result in fluctuations in size and GTPase activity. Nonetheless, our two-parameter analysis identifies other possible mechanisms for the generation of dynamical cellular behaviors. In the original analysis, Zmurchok et al. [32] determined that a cell could transition from a relaxed to oscillatory to contracted state by increasing the feedback strength from tension to GTPase activation through increasing the parameter β. Here, our two-parameter analysis suggests other pathways to generate transitions between the same behaviors. If a cell's ability to respond to mechanical tension is fixed by signalling pathways (i.e., fixed β), then a cell could still generate these behaviors by modulating GTPase translation (increasing or decreasing the parameter b).

We limited our investigation to the $b\beta$-plane, although could expand to other bifurcation parameters of interest. For example, Holmes and Edelstein-Keshet [13] explored the dynamics of similar GTPase signaling models (without feedback from cell mechanics) to that studied here but also examined the role of other parameters such as the total GTPase amount G_T, or the strength of positive feedback, γ, on the dynamics. We briefly

investigated the effect of increasing γ on the bifurcation structure. To avoid the complexity of three simultaneously varying parameters, we fixed b. We found that the region of bistability that encloses the dynamically interesting global bifurcations exists for a wide range of γ for small β. However, as β increased, the region of bistability only exists for a smaller range of γ before the saddle-nodes collide in a cusp bifurcation. Given this observation, we expect the many dynamically interesting bifurcations involving the saddle-node homoclinic solution to persist in parameter space, before being "squeezed" in between the saddle-nodes.

Here, we focused on the key bifurcation parameters and the mathematically and dynamically interesting codimension-two global bifurcations. We confirmed the presence of these global bifurcations in the mechanochemical model using numerical bifurcation software and phase-plane analysis. This analysis provides insight into the joint dynamics of cell signaling and mechanics and provides an example of dynamically interesting global codimension-two bifurcations in a contemporary and realistic mathematical biology model.

Supplementary Information The online version contains supplementary material available at https://doi.org/10.1007/s12591-023-00636-z.

Acknowledgements CZ was partially supported by a Postdoctoral Fellowship Award from the Natural Sciences and Engineering Research Council (NSERC) of Canada and by a National Science Foundation (NSF), United States grant DMS1562078. MS was supported by an Undergraduate Student Research Award (USRA) from NSERC of Canada. WN and ENC are supported by NSERC of Canada.

Data Availability All code used to produce the figures is available as a GitHub repository at https://www.github.com/zmurchok/GTPase-tension-bifurcation.

References

1. Bazykin AD: Nonlinear dynamics of interacting populations. World Scientific Series on Nonlinear Science. Series A: Monographs and Treatises, vol 11. World Scientific Publishing Co., Inc., River Edge, NJ. (1998). https://doi.org/10.1142/9789812798725
2. Bui, J., Conway, D.E., Heise, R.L., Weinberg, S.H.: Mechanochemical coupling and junctional forces during collective cell migration. Biophys. J . **117**(1), 170–183 (2019). https://doi.org/10.1016/j.bpj.2019.05.020
3. Champneys, A.R., Kuznetsov, Y.A., Sandstede, B.: A numerical toolbox for homoclinic bifurcation analysis. Int. J. Bifurcation Chaos **5**, 867–887 (1996). https://doi.org/10.1142/S0218127496000485
4. Chay, T.R., Cook, D.L.: Endogenous bursting patterns in excitable cells. Math. Biosci. **90**(1–2), 139–153 (1988). https://doi.org/10.1016/0025-5564(88)90062-4
5. Chow, S.N., Lin, X.B.: Bifurcation of a homoclinic orbit with a saddle-node equilibrium. Differ. Integral Equ. **3**(3), 435–466 (1990)
6. Chow, S.N., Deng, B., Fiedler, B.: Homoclinic bifurcation at resonant eigenvalues. J. Dyn. Differ. Equ. **2**(2), 177–244 (1990). https://doi.org/10.1007/bf01057418
7. Deng, B.: Homoclinic bifurcations with nonhyperbolic equilibria. SIAM J. Math. Anal. **21**(3), 693–720 (1990). https://doi.org/10.1137/0521037
8. Dhooge, A., Govaerts, W., Kuznetsov, Y.A., Meijer, H.G., Sautois, B.: New features of the software MatCont for bifurcation analysis of dynamical systems. Math. Comput. Model. Dyn. Syst. **14**(2), 147–175 (2008). https://doi.org/10.1080/13873950701742754
9. Farjami, S., Kirk, V., Osinga, H.M.: Transient spike adding in the presence of equilibria. European Phys. J. Special Topics **225**(13), 2601–2612 (2016). https://doi.org/10.1063/1.4826655
10. Friedman, M., Govaerts, W., Kuznetsov, Y.A., Sautois, B.: Continuation of homoclinic orbits in Matlab. In: Lecture Notes in Computer Science, pp. 263–270. Springer, Berlin, Heidelberg (2005). https://doi.org/10.1007/11428831_33

11. Govaerts, W., Sautois, B.: The onset and extinction of neural spiking: a numerical bifurcation approach. J. Comput. Neurosci. **18**(3), 265–274 (2005). https://doi.org/10.1007/s10827-005-0328-9
12. Govaerts W, Witte VD, Kheibarshekan L: Using MatCont in a two-parameter bifurcation study of models for cell cycle controls. In: Volume 4: 7th International Conference on Multibody Systems, Nonlinear Dynamics, and Control, Parts A, B and C. ASMEDC. (2009). https://doi.org/10.1115/detc2009-86185
13. Holmes, W.R., Edelstein-Keshet, L.: Analysis of a minimal Rho-GTPase circuit regulating cell shape. Phys. Biol. **13**(4), 046001 (2016). https://doi.org/10.1088/1478-3975/13/4/046001
14. Homburg, A.J., Sandstede, B.: Homoclinic and heteroclinic bifurcations in vector fields. In: Handbook of Dynamical Systems, pp. 379–524. Elsevier, Amsterdam (2010). https://doi.org/10.1016/s1874-575x(10)00316-4
15. Hoppensteadt, F.C., Izhikevich, E.M.: Bifurcations in neuron dynamics. In: Weakly Connected Neural Networks, pp. 25–101. Springer, New York (1997). https://doi.org/10.1007/978-1-4612-1828-9_2
16. Izhikevich, E.M.: Neural excitability, spiking and bursting. Int. J. Bifurc. Chaos **10**(06), 1171–1266 (2000). https://doi.org/10.1142/s0218127400000840
17. Kuznetsov, Y.A.: Elements of Applied Bifurcation Theory. Springer, Newyork (2004). https://doi.org/10.1007/978-1-4757-3978-7
18. Leontovich, E.: On the generation of limit cycles from separatrices. Doklady Akad. Nauk SSSR (NS) **78**, 641–644 (1951)
19. Levi, M., Hoppensteadt, F.C., Miranker, W.L.: Dynamics of the Josephson junction. Q. Appl. Math. **36**(2), 167–198 (1978). https://doi.org/10.1090/qam/484023
20. Link, P.A., Heise, R.L., Weinberg, S.H.: Cellular mitosis predicts vessel stability in a mechanochemical model of sprouting angiogenesis. Biomech. Model. Mechanobiol. (2021). https://doi.org/10.1007/s10237-021-01442-8
21. Liu, C., Liu, X., Liu, S.: Bifurcation analysis of a Morris-Lecar neuron model. Biol. Cybern. **108**(1), 75–84 (2014). https://doi.org/10.1007/s00422-013-0580-4
22. Lukyanov, V.I.: Bifurcations of dynamical systems with "saddle-node" separatrix loops. Differentsial'nye Uravneniya **18**(9), 1493–1506 (1982)
23. Mori, Y., Jilkine, A., Edelstein-Keshet, L.: Wave-pinning and cell polarity from a bistable reaction-diffusion system. Biophys. J . **94**(9), 3684–3697 (2008). https://doi.org/10.1529/biophysj.107.120824
24. Morris, C., Lecar, H.: Voltage oscillations in the barnacle giant muscle fiber. Biophys. J . **35**(1), 193–213 (1981). https://doi.org/10.1016/s0006-3495(81)84782-0
25. Nozdracheva, V.: Bifurcations of a structurally unstable separatrix loop. Differentsial'nye Uravneniya **18**(9), 1551–1558 (1982)
26. Rajagopal, V., Holmes, W.R., Lee, P.V.S.: Computational modeling of single-cell mechanics and cytoskeletal mechanobiology. Wiley Interdiscip. Rev. Syst. Biol. Med. **10**(2), e1407 (2017). https://doi.org/10.1002/wsbm.1407
27. Ridley, A.J.: Rho family proteins coordinating cell responses. Trends Cell Biol. **11**(12), 471–477 (2001). https://doi.org/10.1016/S0962-8924(01)02153-5
28. Schecter, S.: The saddle-node separatrix-loop bifurcation. SIAM J. Math. Anal. **18**(4), 1142–1156 (1987). https://doi.org/10.1137/0518083
29. Tambyah, T.A., Murphy, R.J., Buenzli, P.R., Simpson, M.J.: A free boundary mechanobiological model of epithelial tissues. Proc. Royal Soci. A Math. Phys. Eng. Sci. **476**(2243), 20200528 (2020). https://doi.org/10.1098/rspa.2020.0528
30. Tsaneva-Atanasova, K., Osinga, H.M., Rieß, T., Sherman, A.: Full system bifurcation analysis of endocrine bursting models. J. Theor. Biol. **264**(4), 1133–1146 (2010)
31. Wilson, H.R., Cowan, J.D.: Excitatory and inhibitory interactions in localized populations of model neurons. Biophys. J . **12**(1), 1–24 (1972). https://doi.org/10.1016/s0006-3495(72)86068-5
32. Zmurchok, C., Bhaskar, D., Edelstein-Keshet, L.: Coupling mechanical tension and GTPase signaling to generate cell and tissue dynamics. Phys. Biol. **15**(4), 046004 (2018). https://doi.org/10.1088/1478-3975/aab1c0